LBL-15133
Preprint

Lawrence Berkeley Laboratory
UNIVERSITY OF CALIFORNIA

Materials & Molecular
Research Division

Submitted to Physical Review B

THE TWO-DIMENSIONAL VALENCE ELECTRONIC STRUCTURE OF A MONOLAYER OF Ag ON Cu(001)

J.G. Tobin, S.W. Robey, and D.A. Shirley

May 1985

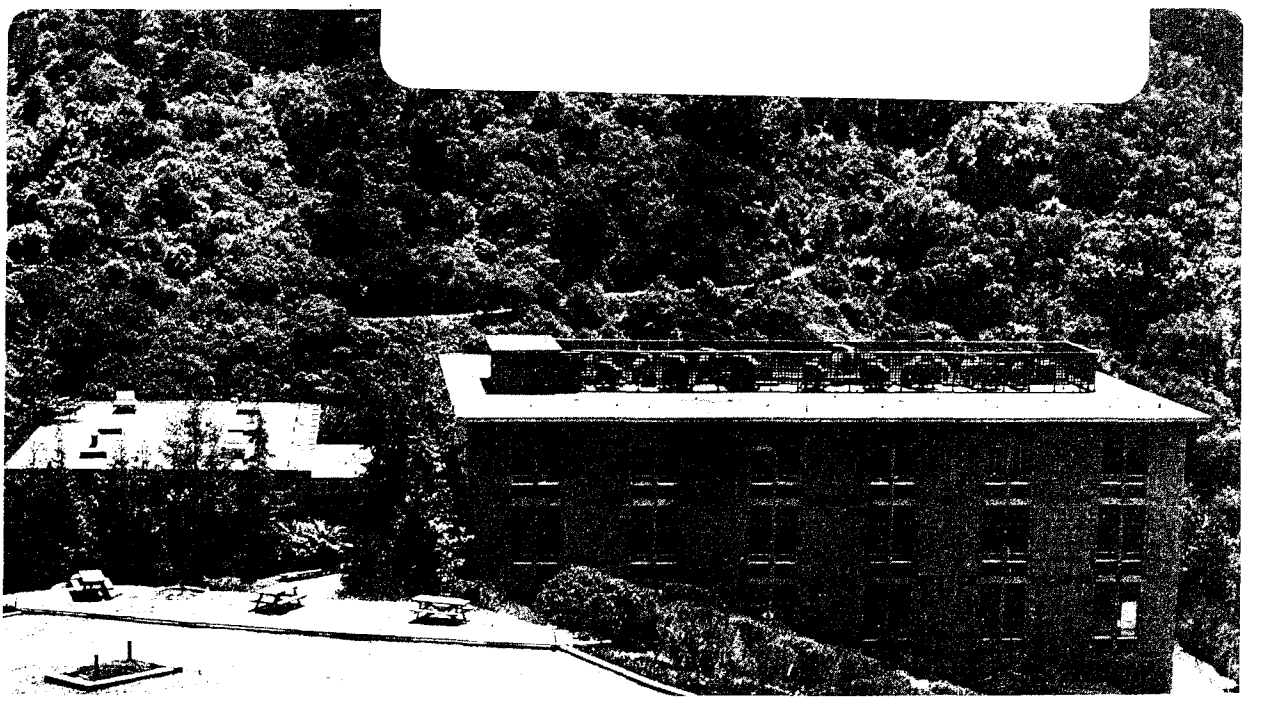

Prepared for the U.S. Department of Energy under Contract DE-AC03-76SF00098

LBL-15133

THE TWO-DIMENSIONAL VALENCE ELECTRONIC STRUCTURE OF A MONOLAYER OF Ag ON Cu(001)

J. G. Tobin*, S. W. Robey and D. A. Shirley

Materials and Molecular Research Division
Lawrence Berkeley Laboratory and the
Departments of Chemistry and Physics
University of California
Berkeley, California 94720

*Permanent address: Department of Chemistry, University of Wisconsin, Madison, Wisconsin 53706.

ABSTRACT

The metal overlayer system c(10x2)Ag/Cu(001) was studied at coverages near one monolayer with angle-resolved photoemission. The observed spectroscopic features indicate a two-dimensional d-band electronic structure that can be interpreted using a model with planar, hexagonal symmetry in which crystal field effects dominate over spin-orbit effects.

I. INTRODUCTION

The electronic structure of metal-monolayer films is a subject of both experimental and theoretical interest. Surfaces consisting of metal overlayers on different metallic substrates have been studied in Angle-Resolved-Photoelectron-Spectroscopy (ARPES) experiments[1-7] and theoretically.[4,6,8-11] Calculations have also been performed to determine the electronic properties of unsupported thin metal slabs.[12-17] This paper gives a detailed account of some of the ARPES results briefly summarized in an earlier Communication.[5] The two-dimensional electronic structure of the overlayer at monolayer coverages, observed using HeI and NeI as the excitation sources, will be discussed. This includes a mapping of the dispersion relations of the overlayer valence bands and the assignment of the observed states on the basis of the polarization dependence of these features.

The system c(10x2)Ag/Cu(001) was chosen for several reasons. Earlier Low Energy Electron Diffraction (LEED) and Auger studies[18] had demonstrated that the c(10x2)Ag was a single, close-packed, hexagonal layer at monolayer exposures. Both the substrate Cu(001)[19] and Ag(111),[20-25] which is the three-dimensional analog of the c(10x2)Ag, have been thoroughly investigated. Silver and copper surfaces are reasonably stable, and Cu(001)[26,27] has a well defined surface state (B^F = 1.8 eV near $\bar{M}$ in the Cu(001) Surface Brillouin Zone) that can be used for surface characterization. Moreover, the valence bands of

Cu(001) and Ag(111) show relatively little overlap in terms of the energy and momentum of the electronic states. Thus the Ag/Cu(001) system held promise as a case study of interfacial electronic structure.

This paper is organized into four more sections. Experimental procedures are described in Section II, and photoemission results are given in Section III. These results are discussed in Section IV, including the framework for determining the two-dimensional dispersion relations and the group-theoretical approach used to establish band symmetries. Conclusions appear in Section V.

II. EXPERIMENTAL

This section has two parts. General procedures are described first, then the LEED/Auger calibration of the sample coverage is treated in detail.

A. GENERAL PROCEDURES

The experiment was performed in an angle-resolved photoelectron spectrometer[27] using a plane-polarized photon beam from a gas discharge lamp. HeI (21.22 eV) and NeI (16.67, 16.85 eV) were used separately as excitation lines. The base pressure was 2×10^{-10} Torr, rising during lamp operation into the 10^{-9} Torr range. Two copper crystals were cut and polished to within ±1° of the (001) crystallographic plane, as determined by Laue backscattering. Both were chemically polished to remove the surface layers. The solution used on the first crystal included HCl[28], while that used on the second did not[29]. Samples were cleaned by continuous Ar ion etching during cycles of heating and cooling at pressures of 10^{-5} Torr, with maximum temperatures of 500-600°C. However, the removal of all evaporated silver, as determined by Auger spectroscopy, was achieved by extended room-temperature sputtering prior to the beginning of cycling. This was done to minimize the danger of alloying. A final anneal to 500-600°C was performed on the cleaned sample to order the surface, as confirmed by LEED. For the annealed surface, the impurity to

copper Auger derivative-peak-height ratios were typically 0.005 or less for carbon, 0.003 or negligible for sulfur, and negligible for oxygen and silver. The success of the cleaning procedure was confirmed by observing the $\bar{M}$ surface state of Cu(001). Similar Auger measurements were also made after the silver exposures and photoemission experiments.

Evaporation was performed with a shielded thermal source of Ag, equipped with a shutter for time control of exposures and a water-cooled quartz crystal microbalance inside the shielding to monitor the evaporation rate. The microbalance was placed closer to the source, to intercept a larger solid angle and give enhanced sensitivity. The pressure rose negligibly during the evaporation operation, generally remaining below the mid 10^{-10} Torr range.

Resolution in the photoemission measurements was determined by a convolution of the source line width (which is negligible), the NeI doublet structure (when applicable) and the analyzer resolution. The analyzer contribution is 0.006 PE, where PE is the pass energy of the hemispherical analyzer. All measurements were taken at either 10 eV, 20 eV, or 40 eV pass energy. At normal emission and polar emission angles, θ_e, of 30° or less, the polar angle of incidence, $\theta_{h\nu}$, of the light was 60° with respect to the normal (Figure 1). For polar photoelectron emission angles larger than 30°, the angle of incidence was such that $\theta_{h\nu} + \theta_e = 90°$. Separate measurements were made with the polarization in the plane of the surface (s-polarization) and in the plane of rotation (p-polarization).

Samples were aligned by laser autocollimation and with LEED. Spectra were taken on both sides of the spectrometer; thus laser autocollimation was performed through several different windows. There is an assumed relative error of ±1° in each alignment, introduced by using different windows or LEED. Intermittent, limited distortion of the LEED patterns and loss of low kinetic energy

electrons in the photoemission spectra were observed. Apparently this was due to charging of the sample plate insulators, particularly after silver exposures.

B. THE LEED/AUGER CALIBRATION

An exact knowledge of the quantity of Ag deposited upon the surface was crucial. While the quartz microbalance should provide a precise relative measure of the amount of evaporation, it was necessary to calibrate the thickness monitor coverage equivalent to one monolayer coverage on the crystal. This was done by making a series of Auger and LEED measurements of surfaces at varied exposures.

A previous experiment performed on the system Ag/Ni(001)[30] demonstrated the validity of a model for systems which grow in a layer-by-layer (Frank-Van Der Merwe) mode. It predicted abrupt changes in the slope of the Auger intensity versus coverage plots at coverages of integral monolayers. Subsequent experimentation has confirmed this in several other systems (Ref. 2 and 3, and references therein).

Owing to the sensitivity of the absolute Auger signal upon the position of the sample relative to the focus of the LEED optics, measurements on this system were made in terms of the ratio of the adsorbate to substrate signals. While this complicates the model slightly by removing the linear dependences, the essential feature of kinks at integral monolayer coverages should be retained. This is confirmed by the results shown in Figure 2, which shows a break-in-slope at $\Delta T' = 40 \pm 5$ Å ($\Delta T'$ is a relative reading taken from the quartz crystal thickness monitor, not an actual thickness. A large proportionality constant was inserted to remove readout error). At slightly greater exposures than that with the discontinuity in the Auger ratio, LEED spots (partial patterns) associated with the c(10x2) structure[18,31] were first observed. Measurements were also made with the Cu 920 eV Auger line.

In a close-packed, slightly-distorted, overlayer which is only weakly in registry with the substrate, ordering might not be expected until the completion of a full monolayer. Thus, the monolayer coverage determination with the Auger measurements is supported by the LEED observations. Both the LEED and Auger results are consistent with a layer-by-layer growth, at least up to near single monolayer coverages. Examples of this type of growth mode would include Frank-Van-Der-Merwe and Stranski-Krastanov growth modes.

In the initial calibration experiment, both orthogonal domains were observed with LEED (Figure 3). The copper crystal used in this and some of the initial clean Cu(001) photoemission measurements displayed a sharp (1x1) LEED pattern and the Cu(001) $\bar{M}$ surface state, but was not of specular quality. Subsequently, a specular quality Cu(001) crystal was substituted. It also displayed a sharp (1x1) LEED pattern, the $\bar{M}$ surface state, and, when exposed to silver, similar Auger ratios, but only one of the two domains was observed with LEED. These results were quite reproducible. Test photoemission spectra were essentially the same for both crystals, both for the clean Cu(001) and for the Ag/Cu(001).

The absence of the second domain has been tentatively explained as follows. As the quality of the crystal preparation improved, any remnant deviation of the crystal face from the Cu(001) plane would become crucial in breaking the degeneracy of the <110> directions. This type of subtle effect might only be noticeable in a specular crystal. Misalignment of a crystal by $\pm 1^\circ$ would produce steps every 57 atoms. Unlike active gas adsorbates which occupy high symmetry sites, the Ag overlayer is a close-packed-structure in which the ordering is susceptible to the influence of steps. This effect may very well provide a means of selectively preparing single domain structures and it warrants further investigation.

In terms of its effect upon photoemission, the presence or absence of the second domain is moot. This follows because the photoelectron originates from an electronic environment which is equivalent in either domain, save for easily accountable azimuthal-directional effects.

Samples of a given coverage were thus prepared. We believe that the one monolayer point was determined with approximately ±10 percent accuracy, but to include the propagation of errors a typical error estimate of ±20 percent will be quoted for all overlayer thickness values. The readings from the quartz microbalance were used as a guide in the evaporation process but actual coverage values were generally determined from the Auger ratio calibration curves and LEED observations. Typically, the agreement was fairly good and the sample preparation was reproducible.

III. PHOTOEMISSION RESULTS

Several measurements were made using samples of clean Cu(001) and c(10x2)Ag/Cu(001) of coverages slightly greater than one monolayer. Photoemission spectra were collected using linearly polarized HeI radiation at 21.22 eV as the excitation and rotating off normal in the (100) and (110) planes of Cu(001), as diagrammed in Figures 1 and 3. The experiment was performed in two configurations, one for s-polarization, the other for p-polarization. In the HeI experiment, the analyzer resolution and the total instrumental resolution were 120 meV FWHM. Photoemission spectra were also collected using polarized NeI radiation at 16.67 and 16.85 eV. Again, separate s- and p-polarization experiments were performed while rotating off normal in the (100) plane of Cu(001). The analyzer resolution in this experiment was 120 meV (c(10x2)Ag/Cu(001)) or 240 meV (clean Cu(001)). Multiplying these contributions with the NeI doublet produces broad, non-gaussian, non-triangular

instrumental lineshapes that are approximately 0.3 eV or 0.4 eV FWHM, respectively. Despite the complication caused by the doublet, the NeI spectra still exhibited relatively sharp, well-defined spectral structure.

As an example of the six data sets described above, let us consider the spectra collected with s-polarized HeI radiation while rotating off-normal in the (100) plane of Cu(001), shown in Figure 4. Several important effects are illustrated by this data set. First, the easily observable silver feature near B^F = 5 eV disperses to higher binding energy with increasing polar emission angle. This will be shown below to be indicative of two-dimensional dispersion. Second, note that this same feature at θ_e = 0° is a flat-topped, broad peak. Below it will be shown to be due to a convolution of two spin-orbit split peaks. Third, the weaker silver feature at B^F near 6 eV is only observable at θ_e above 10°. The appearance of this feature only at angles far off-normal is consistent with the group-theoretical analysis discussed in the next section. Fourth, the $\bar{M}$ surface state of Cu(001) is observed in the clean Cu(001) spectrum at θ_e = 60° (B^F = 1.8 eV) but not in the Ag/Cu(001) spectrum at the same angle. This suggests that the Ag is "wetting" the Cu(001) surface, i.e. there are no open patches of Cu(001) which would give rise to the $\bar{M}$ surface state. Moreover, all of the c(10x2)Ag/Cu(001) spectra at angles of 40° and above show a significant decrease in intensity on the low B^F side of the Cu(001) d-bands. This indicates a strong contribution from surface-derived states to this part of the clean Cu(001) d-band spectral structure at these angles.

The data in Figure 4 are also suggestive of effects that are more strongly encountered in some of the other five data sets.[32] A result of the 23.1 eV He satellite is the weak feature at the apparent $B^F \approx 1.0$ eV in these spectra. Substrate peak distortion and changes in relative intensity are associated

with the silver deposition. There are several possible explanations for this including refraction, mean-free-path variations with kinetic energy, scattering at the interface, binding energy shifts due to the redistribution of charge in the surface dipole layer necessary to equilibrate the Fermi levels in the Cu and Ag, surface resonance coupling of the Cu and Ag states, and physical misalignment on the order of 2°. Of course, increasing the polar emission angle favors emission from the surface region.

Because angle-resolved photoemission is susceptible to these distorting factors, direct subtraction of background spectra proved to be inadequate. However, ARPES allows the actual resolution of separate features, and the background Cu(001) spectra serve as a guide to eliminate substrate peaks. This allows the unambiguous assignment of features to the Ag overlayer. Apparently, the only Ag features lost were those that overlap with the Cu d-bands near B^F = 2 to 3 eV.

Due to the HeI satellite and the weakness of the Fermi edge jump in the s-polarization spectra, averaged values of the spectrometer work function were used to calculate binding energies. The determinations using the p-polarization spectra exhibited a standard deviation of ±0.06 eV or less. This demonstrates the high precision and reproducibility of analyzer element voltage control and measurement. Measurements of the spectrometer work function using the s-polarization spectra were consistent with the above but of lower precision and reliability. The p-polarization values were used for all of the data.

To provide an independent method of confirming the assignments derived from the monolayer data, spectra were also collected from higher coverage samples.[32] Exposures of 2.5 monolayers of silver produced surfaces that also displayed a single c(10x2) LEED pattern. Spectra were collected using HeI radiation while rotating in the (100) plane of Cu(001), making use of s- and

p-polarized light in separate measurements. The silver features were correspondingly stronger and the residual copper features distorted and weaker, in agreement with the previous assignments. (In the synchrotron radiation experiment presented in Ref. 5, and to be detailed in a future publication, normal emission spectra were collected from samples ranging in exposure from one-half to five monolayers. These were also consistent with the above resonance lamp spectra.)

In Figure 5, the binding energies, of all of the observed silver features from the HeI and NeI spectra collected from the near monolayer samples, are plotted versus the parallel component of the crystal momentum, $\vec{k}_{\parallel}$. Even prior to actual assignment of the individual features in the Ag two-dimensional Surface Brillouin Zone (SBZ), several distinct trends in the data can be noted. First, there are four separate sets of states or bands observed in the data based upon polarization and energy dependences. These are labeled i through iv in Figure 5, starting with the most tightly bound. Second, most of these disperse as functions of the parallel component of the crystal momentum, $\vec{k}_{\parallel}$. Third, none show any significant dependence upon the perpendicular component of the crystal momentum, $k_{\perp}$, because the same dispersive relationships are exhibited by the HeI and NeI data. (This is also confirmed by the synchrotron radiation data in Ref. 5 and 32.) Fourth, there is also agreement between the observed polarization dependences for the HeI and NeI data.

The worst disagreement between measurements with different values of $k_{\perp}$ is at $k_{\parallel} \geq 0.8$ Å^{-1} in the <100> surface direction, in the data taken with s-polarized light. The NeI peaks seem to be dispersing downward more rapidly than the HeI data. However, the disagreement can be reconciled by a careful consideration of error propagation. At larger polar emission angles, the NeI features are weaker and more difficult to locate precisely. Thus,

instead of using the usual error estimate of peak position determination, which is a fraction of the peak width, a worst case will be considered which uses FWHM and standard deviation contributions. Of course, binding energy determinations are also ultimately limited by the precision of the determination of the Fermi level.

Using a formalism discussed in the next section, it is possible to estimate the uncertainty of the $k_{||}$ values. The sources of error include the total spectrometer-source energy resolution (discussed above), the uncertainty in the proper work function and angular alignment error. An angular alignment error of ±1° was assumed. A work function error estimate was made by using ϕ = 4.74 eV for Ag(111)[33] as the true or vacuum work function, ϕ = 5.16 eV for Cu(001)[34] as the upper limit and ϕ = 4.3 eV for Ag[33] as the lower limit. The analyzer or spectrometer work function was determined from the photoemission spectra: as discussed above, the average values from the p-polarized spectra were used. The standard deviation of ±0.06 eV was used as the uncertainty in the spectrometer work function. Combining all these produces an uncertainty in $k_{||}$ which is least at θ_e = 0° (normal emission) and increases monotonically with θ_e. For HeI, $\Delta k_{||} = \pm 0.03$ Å^{-1} at θ_e = 0° and $\Delta k_{||} = \pm 0.06$ Å^{-1} at θ_e = 60°. For NeI, the corresponding uncertainties were $\Delta k_{||} = \pm 0.03$ Å^{-1} at θ_e = 0° and $\Delta k_{||} = \pm 0.08$ Å^{-1} at θ_e = 50°. These estimates probably err toward being too large because the uncertainty in the true work function should be treated as a systematic, not random, error. That is, a change in ϕ would shift both curves in the same direction. A more realistic random error estimate would be $k_{||} = \pm 0.03$ Å^{-1} for all the data points. Considering the uncertainty in $k_{||}$ and the total FWHM energy resolution and Fermi energy uncertainty described above, the discrepancy between the HeI and NeI results disappears.

The only other point of apparent inconsistency in the data is the disagreement between the normal emission values for Band i. With the polarization in the $(1\bar{1}0)$ plane, B^F = 6.42 eV, and with it in the (010) plane, B^F = 6.65 eV. This is just barely within the FWHM/standard deviation energy uncertainty estimate and may be indicative of a coupling of a silver state to bulk Cu(001) states. It will be shown below that this state has significant s-character. All other observed features agree within the appropriate energy uncertainty. This strongly suggests that most of the Ag states, in particular the d-states, have no dependence upon $k_\perp$ and that the electronic interaction with the Cu(001) substrate is limited.

Several other comments should be made. First, there is an apparent crossing between Bands ii and iii at the zone boundary $\bar{Z}$. This will be shown to be an avoided crossing in Section IV. Second, there is a strong similarity between the mappings in the <110> and <100> directions, with the possible exception of Band i. Third, the spectra and bandmapping results for 1 ML c(10x2)Ag/Cu(001) bear no resemblance to those of Ag(111).[32,35] The Ag(111) spectra were collected under analogous conditions and in the same spectrometer, at $h\nu$ = 21 eV and $h\nu$ = 14 eV, along the surface Brillouin zone direction $\bar{\Gamma}$ - $\bar{\Sigma}$ - $\bar{M}$. The energies of these bulk states obviously depend very strongly upon $k_\perp$.

Before continuing on to the analysis in the next section, there is a final observation to be made. As a check of our thickness estimates, photoemission intensities of the silver and copper features were compared. Intensities were estimated by fitting the spectra with gaussian peaks and a quadratic background and by a method of background subtraction using the clean Cu(001) spectra. To minimize band and refractive effects, only the normal emission data were used. In going from the 1¼ to the 2½ monolayer exposure,

the Ag/Cu photoemission ratio at $h\nu$ = 21.22 eV increases by a factor of 3.3 ± 0.5. A naively simple model of the photoemission intensities would be to assume the following. The silver intensity is proportional to exposure at low exposures, naively treating all layers the same. The copper intensity would be that of the clean surface attenuated by the overlayer by a factor of $e^{-z/z'}$, with z the film thickness assuming layer-by-layer growth and z' the escape depth of the copper valence photoelectrons through the silver film at normal emission. Assuming a thickness of 2½ Å per silver monolayer and an escape depth of 10 Å for the copper electrons,[36] an increase by a factor of 2.7 is predicted in going from 1¼ to 2½ monolayers. This is quite reasonable agreement with the observed ratio of 3.3 ± 0.5, considering the approximations made.

IV. DISCUSSION

A. DISPERSION RELATIONS AND DIMENSIONALITY

Angle-resolved-photoelectron-spectroscopy allows the resolution of the energy and momentum of the photoelectrons ejected from the material of interest. Working within the direct transition model,[24,37] it is possible to determine the relationship between the energy and crystal momentum in the initial states from which the photoelectrons were removed, i.e. the initial state dispersion relations.

Of crucial importance in this experiment is the dependence or lack of dependence of the dispersion relations of the Ag monolayer valence bands upon the component of the crystal momentum perpendicular to the surface, $\vec{k}_\perp$. Independence of the dispersion relations from $\vec{k}_\perp$ is a necessary condition for a truly two-dimensional electronic structure. Dependence upon $\vec{k}_\perp$ implies either a coupling of the Ag monolayer valence states with those of Cu(001)

or that the monolayer model is incorrect and island formation, interdiffusion, or some other growth mode is being followed.

Of course, independence of the Ag valence band dispersion relations from $\vec{k}_\perp$ is not conclusive evidence for a two-dimensional electronic structure. For that, it is necessary that the energy of the valence bands be dependent upon the parallel component of the crystal momentum, $\vec{k}_{||}$, as well as being independent of $\vec{k}_\perp$.

To make such a determination requires an understanding of the energy and momentum conservations in the photoemission process. Energy conservation requires:

$$h\nu = B^F + KE + \phi = B^F + KE_{AN} + \phi_{AN} \qquad (1)$$

where $h\nu$ is the photon energy, B^F is the binding energy with respect to the Fermi level, KE (KE_{AN}) is the external kinetic energy of the escaping electron with respect to the vacuum (analyzer) and ϕ (ϕ_{AN}) is the true (analyzer or spectrometer) work function. ϕ = 4.74 eV[33] was used as the vacuum work function.

The magnitude of the external electron momentum, $\vec{q}$, can be determined from the external kinetic energy:

$$KE = \frac{\hbar^2 q^2}{2m} \qquad (2)$$

The mass of the electron is designated by m. Using this external momentum and the knowledge of the external electron emission angles, the parallel component of the electron momentum can be determined:

$$\vec{k}^i_{||} = \vec{k}^f_{||} = \vec{q}_{||} = \vec{q} \sin \theta_e \quad , \qquad (3)$$

where θ_e is the external polar emission angle and $\vec{q}_{\parallel}$, $\vec{k}^f_{\parallel}$ and $\vec{k}^i_{\parallel}$ are the components parallel to the surface of the external momentum, the final state crystal momentum and the initial state crystal momentum, respectively. Hence the origins of the various contributions to the uncertainty in $\vec{k}^i_{\parallel}$, discussed in the previous section, are easily seen.

Equation (3) has a number of implied assumptions associated with it. To equate $\vec{q}_{\parallel}$ and $\vec{k}^f_{\parallel}$ requires an absence of surface umklapping[38] in transmission across the interface. To equate $\vec{k}^i_{\parallel}$ and $\vec{k}^f_{\parallel}$ implies that the reciprocal lattice vector involved with the excitation process has a zero magnitude component parallel to the surface. Of course, primary cone emission[39] has been assumed throughout. For comparison, it should be noted that only primary cone emission without surface umklapping is necessary to analyze normal emission of Ag(111).[24,35]

Consideration of the perpendicular components is more involved. Determination of the perpendicular components of these momenta is complicated by the lack of momentum conservation in the transmission across the solid-vacuum interface. The question of perpendicular momentum conservation in the photoemission excitation process is central to this experiment. Thus, energy conservation is used to relate the perpendicular components of the external and final state crystal momenta, i.e. $\vec{q}_{\perp}$ and $\vec{k}^f_{\perp}$. For the sake of testing its validity, it is assumed that the perpendicular component of the crystal momentum is conserved, to within a reciprocal lattice vector, in the excitation process, i.e. $\vec{k}^f_{\perp} = \vec{k}^i_{\perp} + \vec{G}$ with f for the final and i for the initial state.

To test the dependences of the dispersion relations upon $\vec{k}^i_{\perp}$ and $\vec{k}^i_{\parallel}$, the states were mapped versus $\vec{k}^i_{\parallel}$ using two different photon-energy excitation sources, HeI (21.22 eV) and NeI (16.67, 16.85 eV). The difference in photon energies creates two significantly different sets of $k_{\perp}$'s. Moreover, s- and p-polarized light were used in two separate experiments to simplify spectral

assignments and ultimately to gain insight into the symmetry of the potential experienced by the Ag valence states.

The data plotted in Figure 5 indicate a two-dimensional d-band structure. It clearly demonstrates that B^F, the Ag valence band binding energy with respect to the Fermi level, is independent of $\vec{k}_\perp^i$ and dependent upon $\vec{k}_\parallel^i$ for almost all of the data. Band iv may be independent of $\vec{k}_\parallel^i$ as well as $\vec{k}_\perp^i$, suggesting possibly an atomic origin, but the evidence is inconclusive because the data cover such a small $\vec{k}_\parallel^i$ range. The other serious discrepancy is in Band i at normal emission. Based on polarization dependences and the symmetry arguments of the next section, it is believed that these two data points at $\bar{\Gamma}$ originate from an atomic-like Ag5s state. An s state, due to its symmetry and diffuse density cloud, is more likely to interact with the Cu(001) substrate than the more localized d-states. (In the case of Ag/Rh, calculations[10] suggest that the 4d bands of Ag retain their identities as surface states and resonances. Apparently, the Ag5s states are lost in the interaction with the substrate, as with Ag/Pd(001)[6].) As discussed below, the remaining states should have much more d character. Thus this is very strong evidence that a truly two-dimensional electronic structure is present in the Ag d-bands of a monolayer of Ag on top of the Cu(001) substrate. It is also consistent with the behavior observed in the electronic structure of a surface enriched Cu/Ni alloy[40] and the metal overlayer systems Co/Cu[2], Pd/Ag[3], Pd/Nb[4], and Ag/Ni.[7]

B. INITIAL STATE SYMMETRY ASSIGNMENTS

The symmetry assignments of the silver states at the center of the two-dimensional Brillouin zone are shown in Figure 5 and Table I. These were obtained by a consideration of the symmetry of the components of the matrix elements that describe these electronic transitions.[41] The final state

symmetry is known to be of the completely symmetric representation of either the single (small spin-orbit coupling) or the double (large spin-orbit coupling) group representations. The polarization vector of the incoming radiation is either s-polarized (completely parallel to the surface and perpendicular to the plane of rotation) or p-polarized (in the plane of rotation and generally dominated by the component perpendicular to the surface). This leads to a very selective excitation of the Ag initial state electrons, within this model for electronic photoexcitation.

The standard electric dipole approximation[42] was used in analyzing the Ag/Cu polarization dependences. There was no special treatment for surface effects, such as surface photoemission.[41,43] Both the long-wavelength approximation[41,42,43] and the position form[42] of the cross section were utilized. The long-wavelength approximation should hold here because of the generic weak delocalization of d states and the common imperfections in surfaces which break the perfect lateral periodicity of a theoretical lattice. Equating the momentum and position forms of the cross section is useful in determining the transformation properties of the excitation operators.

Working within the above approximations, the polarization dependences of the Ag bands are easily explained by a simple physical model assuming a small spin-orbit effect (single groups) and a C_{6v} symmetry potential with a small delocalization perturbation. This implies several important results: (1) except for the copper breaking the mirror symmetry parallel to the surface plane and possible static shifts of the Ag levels, the isolated-hexagonal-monolayer picture is accurate; (2) spin-orbit effects are smaller and less important than crystal-field splittings; (3) the Ag4d electrons are very localized; and (4) the spin-orbit splitting of two-dimensional Ag4d electrons is the same as that observed in the free atom and three-dimensional bulk Ag(111). This will be discussed in more detail below.

First, the assignments at the center of the surface Brillouin zone will be discussed; i.e., normal emission results. These are summarized in Table I. The physical model of a monolayer of c(10x2)Ag/Cu(001) is that of a slightly-strained (±2%) hexagonal overlayer. At normal emission, $\vec{k}_{\parallel}^{i} = 0$ and atomic and nearest neighbor effects should dominate. It is also assumed that the interaction of the overlayer with the substrate is limited: $\vec{k}_{\perp}^{i}$ is meaningless, the copper substrate serves to break the surface in-plane mirror symmetry and statically shift the Ag valence states, and the corrugation effects from the four-fold (001) surface can be ignored. This would give rise to a potential of C_{6v} symmetry. Using this approach, the normal emission data can be explained.

The absent feature near $B^F = 5.7$ eV corresponds to the forbidden transition from the E_2 ($d_{x^2-y^2}$ and d_{xy}) states. The flat-topped feature observed near $B^F = 4.8$ eV with s-polarized and p-polarized radiation arises from the spin-orbit split E_1 (d_{xz} and d_{yz}) states, which will be considered below. Finally, the features observed with p-polarized radiation near $B^F = 4.2$ eV and $B^F = 6.5$ eV are due to the A_1 states. The 5s state should be the most tightly bound at the center of the surface Brillouin zone. The other A_1 state (at $B^F = 4.2$ eV) is the $d_{3z^2-r^2}$ state.

Next, the off-normal results will be considered. These states should be more strongly delocalized and hybridized mixtures of s and d states. At off-normal emission, $\vec{k}_{\parallel}^{i}$ will be nonzero and the C_{6v} potential may be perturbed by the effects of delocalization. In the $\bar{\Gamma}$-$\bar{M}$ and $\bar{\Gamma}$-$\bar{K}$ directions of the Ag two-dimensional surface Brillouin zone (Figure 3), this would be of C_s symmetry, since they are in mirror planes. For the $\bar{\Gamma}$-$\bar{Z}$ direction, it will be approximately C_s near $\bar{\Gamma}$ and become C_1 near $\bar{Z}$. (This is supported by the similarity of the mappings near $\bar{\Gamma}$ in both directions shown in Figure 5.)

From the experimental results in the C_s symmetry regions, the only major change from the C_{6v} selection rules at $\bar{\Gamma}$ is the breaking of the forbiddenness of the Band ii transition. (The observation of Band ii at $k_{||} > 0$ with p-polarization may be due to surface photoemission.) Otherwise, the C_s perturbation is not significant. For example, if the C_s perturbation were strong, Bands ii and iii would each split into two bands. Each pair of bands would have one which would be excited by s-polarization and one excited by p-polarization. This suggests the degree of delocalization of the bands, particularly the 4d components, is limited. This dominance of nearest-neighbor-effects upon the selection rules may reflect the same localization of the d-levels that may be contributing to the strong atomic nature of bulk Ag cross section angular dependences.[44]

The effect of the C_1 perturbation can be seen in the changes of the polarization dependences as $k_{||}^i$ approaches $\bar{Z}$, particularly the loss of selectivity for Band i. Note the C_1 symmetry means that Bands ii and iii should have an avoided crossing at $\bar{Z}$. However, if the potential was still purely C_{6v}, then Bands ii and iii could be allowed to cross.

The other major potential perturbation is that due to spin-orbit splitting. In bulk Ag(111),[24] the crystal field splitting (10 Dq = 0.865 ± 0.027 eV) and the spin-orbit contribution (ξ(4d) = 0.232 ± 0.011 eV) are of roughly the same magnitude. In a qualitative sense, the impact of the spin-orbit splitting would seem to be increased by the very high symmetry of the octahedral potential in an FCC crystal. Note that octahedral corresponds to a spherical limit while C_{6v} symmetry would correspond to $C_{\infty v}$. Because of the lowered symmetry of the overlayer and the apparent uniformity of the spin-orbit splitting parameter (the atomic value is ξ(4d) = 0.224 eV[45]), it might be expected that the spin-orbit effect be less important in the Ag monolayer. In fact, this is observed. The only measurable consequence of the spin-orbit perturbation is

the broadening of the Band iii, E_1 peak at normal emission. The spin-orbit interaction may be a source of broadening in the off-normal peaks also.

The measured splitting is ξ(2D-Ag4d) = 0.24 ± 0.06 eV. This is in reasonable agreement with the values for Ag(111) and atomic Ag. The results of fitting the normal emission E_1 peak are summarized in Table II. Note that this feature was also observed with p-polarization due to its parallel component of polarization.

Finally, the effect of the 2% compression/expansion will be considered. It is important that the surface area per Ag atom is essentially the same in an unperturbed Ag(111)-like layer and a layer of c(10x2)Ag.[7] Also, the c(10x2)Ag probably has a range of vertical displacements to lessen the effect of the horizontal strain. This, of course, is an option limited to a surface layer. These two factors seem to militate against any concern about spectral effects of strain such as those observed in condensed materials under high pressures.[46]

C. COMPARISON WITH MONOLAYER CALCULATIONS

It is also useful to compare the results of this experiment with the calculations of the valence electronic structure of a free monolayer of Cu(111).[16] Both Ag and Cu are Column IB metals and the Ag overlayer does appear to be perturbed only weakly by the copper substrate. Hence, the comparison should be a useful exercise.

The results of the Linear-Augmented-Plane-Wave calculations are summarized in Figure 5 of Ref. 16a and Figure 1 of Ref. 16b. The reflection symmetry into the plane of the slab will be used to relate the experimental to theoretical bands. Band iii of this paper is the doubly degenerate (at $\bar{\Gamma}$) odd band in Ref. 16a and 16b. Band ii corresponds to the doubly degenerate (at $\bar{\Gamma}$) even

band in Ref. 16a and 16b. Bands iv and i are each singly-degenerate even bands in Ref. 16a and 16b, with Band i the more tightly bound of the two.

There are major disagreements for the mapping along $\bar{\Gamma}\bar{\Sigma}\bar{M}$ ($k_{\parallel}$ <110> in Figure 5 of this paper). The first is that, in Ref. 16a and 16b, each of the doubly degenerate bands splits as it moves from $\bar{\Gamma}$ toward $\bar{M}$. The second is that Band iv is not located above Bands i, ii and iii. In Ref. 16a, it is between Bands i and ii at $\bar{\Gamma}$ and in Ref. 16b it is between Bands ii and iii at $\bar{\Gamma}$. There may be, however, an explanation for these discrepancies.

The LAPW methods may have overemphasized interactive effects. The magnitude of the experimentally observed C_s perturbation, which is a measure of the delocalization, is limited. In this work, neither Band ii nor iii is observed to split along $\bar{\Gamma}\bar{\Sigma}\bar{M}$, away from $\bar{\Gamma}$. Also, in Ref. 16a and 16b, Band iv could have been drawn down via an interaction with Band i. These disagreements could be due to an overemphasis of delocalization and interband hybridization by the LAPW methods. These effects might disappear under a tight-binding approximation method, but the fact that Ref. 16b carried its calculation to self-consistency argues against it. However, Ref. 16b does demonstrate a shift in Band iv upward relative to Ref. 16a. This may reflect improvements in going from non-self-consistency to self-consistency. Otherwise, the results of Ref. 16a and 16b are almost identical, and display the same discrepancies with this work.

Another possibility is that perhaps the inclusion of a substrate could improve the agreement. For example, hybridization or mixing of the A_1 states (Ag5s and Ag4d $_{3z^2-r^2}$) may be affected by the interaction of the Ag5s states with the substrate, discussed below. Additionally, a strong interaction

between the Ag5s states and the substrate could disrupt the usual hybridization due to the crossing of the rapidly dispersing sp band with the less dispersive d bands, away from $\bar{\Gamma}$.

On the other hand, there are some intriguing similarities in the mappings along $\bar{\Gamma}\bar{\Sigma}\bar{M}$ of this experiment and Ref. 16a and 16b. Band i rises and bends over along $\bar{\Gamma}\bar{\Sigma}\bar{M}$ in all of these works. Band ii disperses upward and Band iii disperses downward in all. Also, Band iv is approximately flat near $\bar{\Gamma}$ in all three cases. (The range of data from this work is very limited for Band iv.) Lastly, there are strong similarities in the mappings along $\bar{\Gamma}\bar{\Sigma}\bar{M}$ and $\bar{\Gamma}\bar{T}\bar{K}$ in Ref. 16a and 16b as there are resemblances between the mappings along $\bar{\Gamma}\bar{\Sigma}\bar{M}$ ($k_{\|}$<110>) and $\bar{\Gamma}\bar{Z}$ ($k_{\|}$<100>) in this work. That is, the bands disperse isotropically, moving away from $\bar{\Gamma}$.

Hence, despite an apparent over-accentuation of interaction effects in Ref. 16a and 16b, qualitatively the dispersion of each individual band is the same in those calculations and this experiment.

D. CRYSTAL FIELD SPLITTINGS

At the center of the Brillouin zone, the energy separations between d-states should reflect the contributions from crystal field and spin-orbit splittings. At this point in the Brillouin zone, atomic and nearest-neighbor perturbations should rival or even dominate delocalization effects. Empirically, this approach has proven successful in the analysis of the splittings of the d-manifold at the center of the bulk Brillouin zone, Γ, in the FCC crystals Ag(111)[24], Au(111)[47] and Pt(111).[47]

However, the success of this procedure may be due in part to a fortuitous cancellation of overlap terms. A calculation of the d-state overlap parameters in an Extended-Hückel treatment of copper surfaces[48] and a generalized consideration of the Hückel theory[49] have demonstrated this cancellation.

Regardless of the source of the success of this method, it should be useful to apply it to the electronically two-dimensional system c(10x2)Ag/Cu(001). As in Section B above, a single group approach will be utilized and any perturbation from the underlying copper substrate will be ignored, save for the breaking of the mirror symmetry parallel to the surface.

Thus, consider the effect of the nearest-neighbors in a ligand-field scheme, within this simplistic model. It is possible to predict independently the ordering of the C_{6v} states of L=2 origin at $\bar{\Gamma}$, and, conceivably, to scale splittings from the known, bulk, L=2, crystal field splitting of Ag(111). At Γ and $\bar{\Gamma}$, the appropriate spherical harmonic wavefunctions can be used to calculate the relative splittings within the d-manifold. Taylor series expansions,[32,50] of the Coulombic potentials associated with the nearest

neighbors, in a FCC octahedral lattice and in a C_{6v} hexagonal planar array, were performed. The following effective potentials were used.

$$V_{\substack{FCC \\ OCT}} = \frac{-35}{8}\frac{e}{a^5}\left(\frac{-3}{5}r^4 + x^4 + y^4 + z^4\right) \tag{4}$$

$$V_{HEX} = \frac{-3}{2}\frac{e}{a^3}\left(3z'^2 - r^2\right) \tag{5}$$

Because of the approximate nature of this approach, only the lowest order, non-constant terms were included. Here -e is the charge of an electron, a is the nearest neighbor distance, and $\hat{x} = [100]$, $\hat{y} = [010]$, $\hat{z} = [001]$ in (4) and $\hat{z}' = \frac{[111]}{\sqrt{3}}$ of bulk Ag in (5). Calculating the expectation values for the E_g and T_{2g} states of Ag(111) and the states of the Ag hexagonal layer, the ordering and splitting shown in Figure 6 were obtained.

It is of interest that the ordering agrees perfectly with that found spectroscopically. Also, the total splitting in the hexagonal case should be larger than in the octahedral. This is because $\langle r^2\rangle/a^2$ should be greater than $\langle r^4\rangle/a^4$, since $\langle r^n\rangle/a^n \cong (\langle r\rangle/a)^n$ and $\langle r\rangle \lesssim \frac{1}{2}a$. This supports the assertion made above of the dominance of the crystal field splitting and the appropriateness of the single group analysis.

A quantitative consideration of the splitting is hampered by a lack of applicable radial expectation values. The use of atomic expectation values[51] produces unphysical results. In fact, the $\langle r^2\rangle$ value calculated from the splitting of the y_2^0 and $y_2^{\pm 1}$ states is significantly different than the atomic value: $(\langle r^2\rangle_{exp})^{\frac{1}{2}} \tilde{=} \frac{1}{2}a$ while $(\langle r^2\rangle_{Ref.\ 51})^{\frac{1}{2}} \tilde{=} \frac{1}{4}a$. Nevertheless, the ratio of the experimental splittings between the d-states at $\bar{\Gamma}$ can be estimated and compared to these crude theoretical predictions. Performing a linear extrapolation of Band ii back to $\bar{\Gamma}$, the ratio of the splitting of the $Y_2^{\pm 1}$-$Y_2^{\pm 2}$ states to that of the Y_2^0-$Y_2^{\pm 1}$ states is roughly 3/2. Considering the extent of the approximations, this is fair agreement with the predicted value of 3.

V. CONCLUSIONS

It has been shown by angle-resolved-photoemission that the d-bands of a monolayer of c(10x2)Ag/Cu(001) are electronically two-dimensional. The d-bands of the silver monolayer clearly show dispersion in the overlayer plane ($k_{||}$) and a lack of dispersion in the direction along the surface normal ($k_{\perp}$). It appears that a state with strong s-character may be interacting with the Cu(001) substrate. The experimental photoemission features can be assigned upon the basis of C_{6v} selection rules with the use of single group representations. Delocalization of the 4d electrons is sufficient to produce two-dimensional dispersion but in general the selection rules are dominated by the nearest-neighbor-symmetry perturbation. A comparison with LAPW calculations for a (111) monolayer showed only limited agreement. A simple model predicts accurately the observed ordering of the L=2 states at $\bar{\Gamma}$ but a full quantitative analysis is not possible at this time. The spin-orbit splitting parameter is found to agree reasonably well with those observed in atomic and bulk systems.

Concerning the nature of overlayer-substrate bonding, a pattern is developing in the case of Ag monolayers on a variety of substrates. In general, the Ag 5s states are active in the interfacial bonding. For Ag/Cu(001), this is suggested by the results of this work and further evidence will be presented in a future publication dealing with the development of electronic three-dimensionality in the metal overlayer film. As mentioned above, the experiments and calculations for the system Ag/Pd(001)[6] indicate a strong interaction for states with Ag 5s character and the Ag/Rh calculations[10] also suggest, by omission, that the Ag 5s states lose their surface identity in the process of adhesion. (Unfortunately, since neither polarization studies nor calculations were performed for the Ag/Ni systems[7], it is difficult to separate the s and d character of the bands. Hence the Ag/Ni studies will not be considered in this discussion of the bonding contributions of the Ag 5s states.)

In the case of the Ag 4d levels, the situation is entirely different. Preliminary results suggest that epitaxial growth is necessary for interfacial bonding to occur via the Ag 4d states. In the case of c(10x2)Ag/Cu(001), a commensurate but non-epitaxial growth pattern occurs. For Ag/Ni(001) and Ag/Ni(111), incommensurate growth patterns are observed. All three have a six-fold symmetric, Ag(111)-like monolayer structure. Despite being unable to assign the symmetry of the Ag states in the Ag/Ni systems, there are strong, obvious similarities between the Ag/Ni and Ag/Cu(001) results. This is particularly true of some of the regions of the Ag/Cu(001) band mapping which are dominated by d-character, i.e. Bands ii and iii of Ag/Cu(001). These results, taken together, suggest that the interaction of the Ag 4d states with the Cu and Ni substrates is very limited.

However, for systems which exhibit epitaxial growth, there is a strong Ag 4d interaction with the substrate. The Ag/Pd(001) study indicates that the Ag4d's are actively involved in the bonding across the interface. The Ag/Rh work suggests that strong enough overlap occurs to cause the 4d's to become partial surface resonances instead of always remaining surface states.

There is, however, a fundamental flaw in these arguments. The interaction may be a matter of overlap in energy and k-space. In the spectroscopic measurements presented here, Ag peaks which overlapped strongly with the Cu bands could be lost. Thus, the focus of the measurements is skewed toward the non-overlapping sections of the Ag bands. (Overlap in terms of B^F and θ_e is not quite the same as in terms of B^F and $\vec{k}$ but considering the uncertainty of the shape and size of the surface potential, it is a reasonable first approximation.) Also, measurements were limited to high-symmetry directions. Hence, significant extensions of both theory and experiment must occur before an understanding is obtained of even the rather limited case of interfacial bonding in Ag overlayers on single crystal metal substrates.

ACKNOWLEDGMENTS

We wish to acknowledge Mrs. Winifred Heppler for the preparation of the copper crystals and D. J. Trevor, C. C. Bahr, and J. J. Barton for their programs used in data reduction. Discussions with R. F. Davis and M. G. Mason were enlightening and greatly appreciated. We also wish to thank L. Kleinman for pointing out the results of the Hückel calculations and T.-C. Chiang for providing the Ag/Ni results prior to publication.

This work was supported by the Director, Office of Energy Research, Office of Basic Energy Sciences, Chemical Sciences Division of the U.S. Department of Energy under Contract No. DE-AC03-76SF00098. One of us (J.G.T.) acknowledges support by an NSF fellowship.

REFERENCES

1. P. Heimann, H. Neddermeyer, and H. F. Roloff, Proc. 7th Intern. Vac. Cong. and 3rd Intern. Conf. Solid Surfaces at Vienna, 2145 (1977).
2. R. Miranda, F. Yndurain, D. Chandesris, J. Lecante, and Y. Petroff, Phys. Rev. B 25, 527 (1982); Surf. Sci. 117, 319 (1982); R. Miranda, D. Chanderis and J. Lecante, Surf. Sci. 130, 269 (1983).
3. G. C. Smith, C. Norris, C. Binns and H. A. Padmore, J. Phys. C: Solid State Phys. 15, 6481 (1982).
4. M. El-Batanouny, D. R. Hamann, S. R. Chubb and J. W. Davenport, Phys. Rev. B 27, 2575 (1983); M. El-Batanouny, M. Strongin and G. P. Williams, Phys. Rev. B 27, 4580 (1983).
5. J. G. Tobin, S. W. Robey, L. E. Klebanoff and D. A. Shirley, Phys. Rev. B 28, 6169 (1983).
6. T. W. Capehart, R. Richter, J. G. Gay and J. R. Smith, Bull. of the APS, 29, 525 (1984); T. W. Capehart, R. Richter, J. G. Gay, J. R. Smith, J. C. Buchholz and F. J. Arlinghaus, J. Vac. Sci. Technol. A1, 1214 (1983).
7. A. P. Shapiro, A. L. Wachs, T. Miller and T.-C. Chiang, unpublished preprint and Bull. of the APS 30, 221 (1985).
8. J. Tersoff and L. M. Falicov, Phys. Rev. B 25, 2925 (1982).
9. D.-S. Wang, A. J. Freeman, H. Krakauer, Phys. Rev. B 26, 1340 (1982); S. Ohnishi, M. Weinert and A. J. Freeman, Phys. Rev. B 30, 36 (1984).
10. P. J. Feibelman and D. R. Hamann, Phys. Rev. B 28, 3092 (1983).
11. P. D. Loly and J. B. Pendry, J. Phys. C 16, 423 (1983).
12. B. R. Cooper, Phys, Rev. Lett. 26, 1316 (1973).
13. G. S. Painter, Phys. Rev. B 17, 3848 (1978).
14. C. S. Wang and A. J. Freeman, Phys. Rev. B 18, 1714 (1978).
15. F. J. Arlinghaus, J. G. Gay and J. R. Smith, Phys. Rev. B 20, 1332 (1979); Phys. Rev. B 25, 643 (1982).

16. a. O. Jepsen, J. Madsen and O. K. Andersen, Phys. Rev. B 18, 605 (1978).
b. E. Wimmer, J. Phys. F.: Metal Phys. 14, 2613 (1984).
17. A. Euceda, D. M. Bylander and L. Kleinman, Phys. Rev. B 28, 528 (1983).
18. P. W. Palmberg and T. N. Rhodin, J. Appl. Phys. 39, 2425 (1968); J. Chem. Phys. 49, 134 (1968); 49, 147 (1968).
19. J. A. Knapp, F. J. Himpsel and D. E. Eastman, Phys. Rev. B 19, 4952 (1979).
20. N. E. Christensen, Phys. Stat. Sol. (B) 54, 551 (1972).
21. H. F. Roloff and H. Neddermeyer, Solid State Comm. 21, 561 (1977).
22. G. V. Hansson and S. A. Flodstrom, Phys. Rev. B 17, 473 (1978).
23. D. Liebowitz and N. J. Shevchik, Phys. Rev. B 17, 3825 (1978).
24. P. S. Wehner, R. S. Williams, S. D. Kevan, D. Denley and D. A. Shirley, Phys. Rev. B 19, 6164 (1979).
25. D. P. Spears, R. Melander, L. G. Petersson and S. B. M. Hagstrom, Phys. Rev. B 21, 1462 (1980).
26. P. Heimann, J. Hermanson, H. Miosga, and H. Neddermeyer, Phys. Rev. Lett. 42, 1782 (1979); Phys. Rev. B 20, 3059 (1979).
27. S. D. Kevan and D. A. Shirley, Phys. Rev. B 22, 542 (1980).
28. G. Petzow, "Metallographic Etching", Amer. Soc. for Metals, 1978; page 59, chemical polish Number 1.
29. W. J. M. Tegart, "The Electrolytic and Chemical Polishing of Metals", Pergamon, 1959; page 100, modified solution.
30. D. C. Jackson, T. E. Gallon and A. Chambers, Surf. Sci. 36, 381 (1973).
31. E. Bauer, Surf. Sci. 7, 351 (1967).
32. J. G. Tobin, Ph.D. Thesis, University of California, Berkeley, 1983, LBL-14704.
33. J. Hölzl, F. K. Schulte and H. Wagner, "Solid Surface Physics", Springer-Verlag, 1979.

34. Z. Hussain, S. Kono, L.-G. Petersson, C. S. Fadley and L. F. Wagner, Phys. Rev. B 23, 724 (1981).

35. J. G. Nelson, S. Kim, W. J. Gignac, R. S. Williams, J. G. Robin, S. W. Robey and D. A. Shirley, LBL-15135, unpublished.

36. P. S. Wehner, Ph.D. Thesis, University of California, Berkeley, 1978, unpublished; C. R. Brundle, J. Vac. Sci. Technol. 11, 212 (1974).

37. Z. Hussain, E. Umbach, J. J. Barton, J. G. Tobin and D. A. Shirley, Phys. Rev. B 25, 672 (1982).

38. J. F. Van Der Veen, F. J. Himpsel and D. E. Eastman, Phys. Rev. B 22, 4226 (1980) and references therein.

39. G. D. Mahan, Phys. Rev. B 2, 4334 (1970).

40. P. Heimann, J. Hermanson, H. Miosga and H. Neddermeyer, Sol. State Comm. 37, 519 (1981).

41. J. Hermanson, Sol. St. Comm. 22, 9 (1977); M. Scheffler, K. Kambe and F. Forstmann, Sol. St. Comm. 25, 93 (1978); and references therein of each.

42. C. Cohen-Tannoudji, B. Diu and F. Laloe, "Quantum Mechanics", Wiley, 1977, p. 1304.

43. H. J. Levinson, E. W. Plummer and P. J. Feibelman, Phys. Rev. Lett. 43, 952 (1979).

44. R. F. Davis, S. D. Kevan, B.-C. Lu, J. G. Tobin and D. A. Shirley, Chem. Phys. Lett. 71, 448 (1980).

45. L. Ley, S. P. Kowalzyk, F. R. McFeely and D. A. Shirley, Phys. Rev. B 10, 4881 (1974).

46. H. G. Drickamer, Intern. Rev. in Phys. Chem. 2, 171 (1982).

47. K. A. Mills, R. F. Davis, S. D. Kevan, G. Thornton and D. A. Shirley, Phys. Rev. B 22, 581 (1980).

48. D. G. Dempsey and L. Kleinman, Phys. Rev. B 16, 5356 (1977).

49. Philip W. Anderson, Phys. Rev. 181, 25 (1969).

50. M. Tinkham, "Group Theory and Quantum Mechanics", McGraw-Hill, 1964, pp. 68-69.

51. T. A. Carlson, C. C. Lu, T. C. Tucker, C. W. Nestor, F. B. Malik, "Eigenvalues, Radial Expectation Values and Potentials for Free Atoms From Z=2 to 126 as Calculated from Relativistic Hartree-Fock-Slater Atomic Wavefunctions", Oak Ridge National Laboratory, ORNL 4614.

TABLE CAPTIONS

Table I Assignments at $\bar{\Gamma}$ of the hexagonal surface Brillouin zone of c(10x2)Ag/Cu(001).

Table II Normal emission data for Band iii, including both s- and p-polarization features. The p-polarized radiation also had a nonzero component of polarization parallel to the surface. The values of B^F were determined by visual inspection. From these, a spin-orbit splitting was determined, ΔB_1^F. ΔB_2^F was determined from fitting each feature with two lorentzian peaks and a linear background. The average spin-orbit-splitting is also shown.

Table I. Assignments at $\bar{\Gamma}$, the center of the surface Brillouin zone.

Band	C_{6v} representation	Spherical harmonics	Orbitals
iv	A_1	y_2^0	$d_{3z^2-r^2}$
iii	E_1	$y_2^{\pm 1}$	d_{xz}, d_{yz}
ii	E_2	$y_2^{\pm 2}$	$d_{x^2-y^2}$, d_{xy}
i	A_1	y_0^0	s

Table II. Spin orbit splitting at the 2D SBZ center ($k_{\|} = 0.00$ Å^{-1}).

	Polarization	Azimuth	B^F (eV)		ΔB_1^F (eV)	ΔB_2^F (eV)
HeI	s	(100)	4.66	4.91	0.25	0.30
NeI	s	(100)	4.64	4.79	0.15	0.28
HeI	s	(110)	4.71	4.87	0.16	0.23
HeI	p	(100)	4.71	4.91	0.20	0.29
NeI	p	(100)	4.73		--	0.33
HeI	p	(110)	4.73	4.97	0.24	0.17
Average			4.69	4.89	0.20	0.27
Standard Deviation			0.04	0.07	0.05	0.06

Spin Orbit Splitting = 0.24 ± 0.06 eV.

FIGURE CAPTIONS

Figure 1. Schematic of the vectoral geometry of the ARPES experiments. The Cu(001) normal, the Poynting vector of the light and the center line of the analyzer acceptance cone are all in the horizontal plane. For p-polarization, the polarization is also in the horizontal plane. In the case of s-polarization it is perpendicular to the horizontal plane.

Figure 2. Plot of the derivative intensity ratio of the Ag MNN Auger line at 350 eV to the Cu MVV Auger line at 60 eV versus readings from the quartz microbalance thickness monitor. $\Delta T'$ is a relative reading and should not be construed as an actual thickness.

Figure 3. A depiction of a model of one of the two orthogonal domains of c(10x2)Ag/Cu(001) in real space. The centers of the silver atoms are represented by filled circles and the centers of the Cu atoms by intersecting lines. The c(10x2) is a slightly strained (±2 percent) hexagonal structure. The actual registry with the substrate is unknown. The Surface Brillouin Zones of Cu(001) and both undistorted hexagonal c(10x2)Ag domains are shown. Also included are the paths taken across each zone when rotating off-normal in the Cu(001) planes (110) and (100). Only the domain associated with (c) was observed with LEED. Rotating off normal in the (100) plane, the same direction is taken in both Ag domains. The hexagonal-zone boundary in this direction has been arbitrarily called $\bar{Z}$.

Figure 4. Spectra taken of clean Cu(001) (lower member of each pair) and 1¼ monolayers of c(10x2)Ag/Cu(001) (upper member of each pair), with s-polarized HeI radiation. Analyzer and total resolution is 120 meV. The HeI satellite at 23.1 causes the small structure near the Fermi edge. These spectra were taken rotating away from the normal in the (100) plane, with the polarization in the (001) or surface plane. The light polarization and electron emission direction are separated by 90°. The angle listed is the polar emission angle (θ_e) versus the surface normal. Each spectrum is normalized to the largest Cu d-band peak.

Figure 5. Map of binding energy versus $k_{||}$, in two directions across the Surface Brillouin Zone of c(10x2)Ag, as shown in Figure 3. Table II contains a summary of the binding energies used to calculate the average values near B^F = 4.8 eV.

Figure 6. Crystal field splitting in a d-manifold predicted for a FCC octahedral field caused by 12 nearest neighbors and for a hexagonal C_{6v} field caused by six in-plane nearest neighbors. Only the first non-constant term from each expansion was used. The scaling of the splittings corresponds to those found experimentally in Ag(111) (Ref. 24) and c(10x2)Ag/Cu(001). A factor of e^2/a must be included to obtain the splittings in terms of energy units.

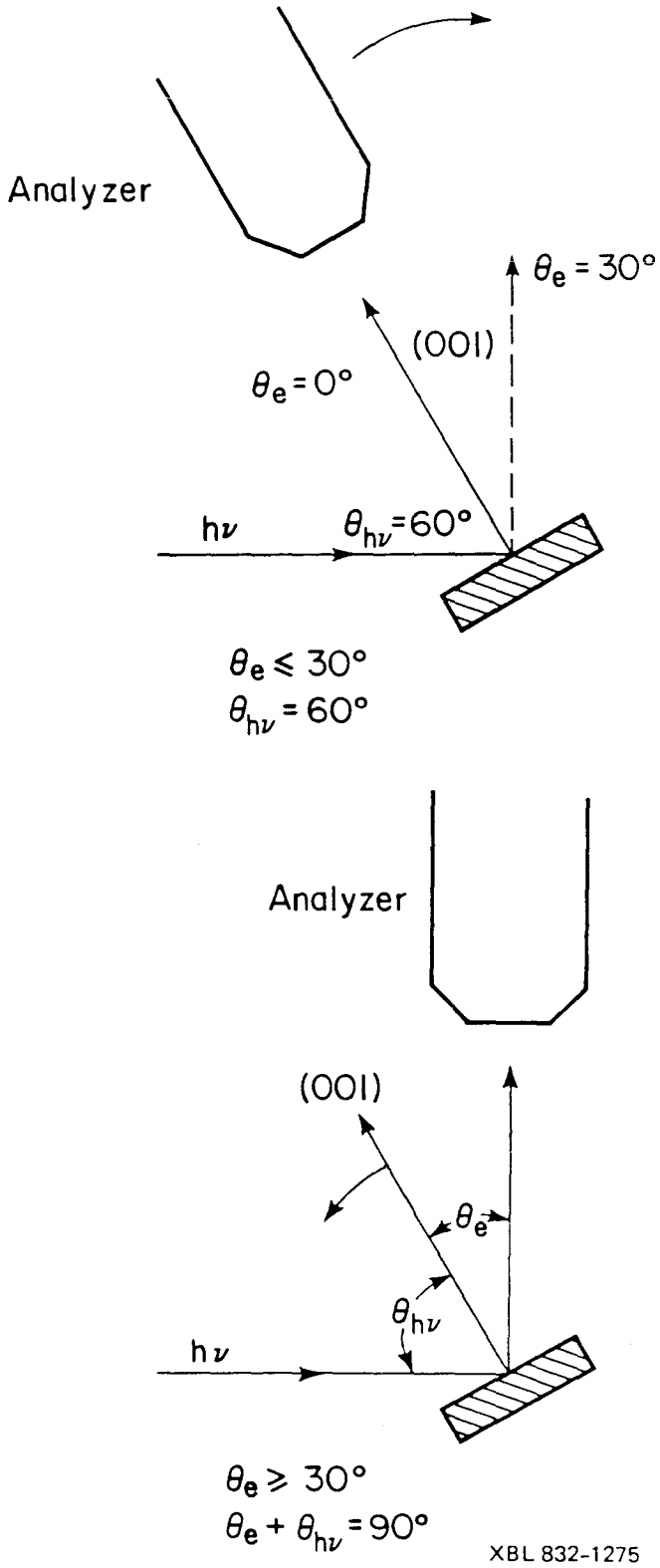
Analyzer
$\theta_e = 30°$
(001)
$\theta_e = 0°$
$h\nu$
$\theta_{h\nu} = 60°$
$\theta_e \leq 30°$
$\theta_{h\nu} = 60°$
Analyzer
(001)
θ_e
$\theta_{h\nu}$
$h\nu$
$\theta_e \geq 30°$
$\theta_e + \theta_{h\nu} = 90°$
XBL 832-1275

Figure 1

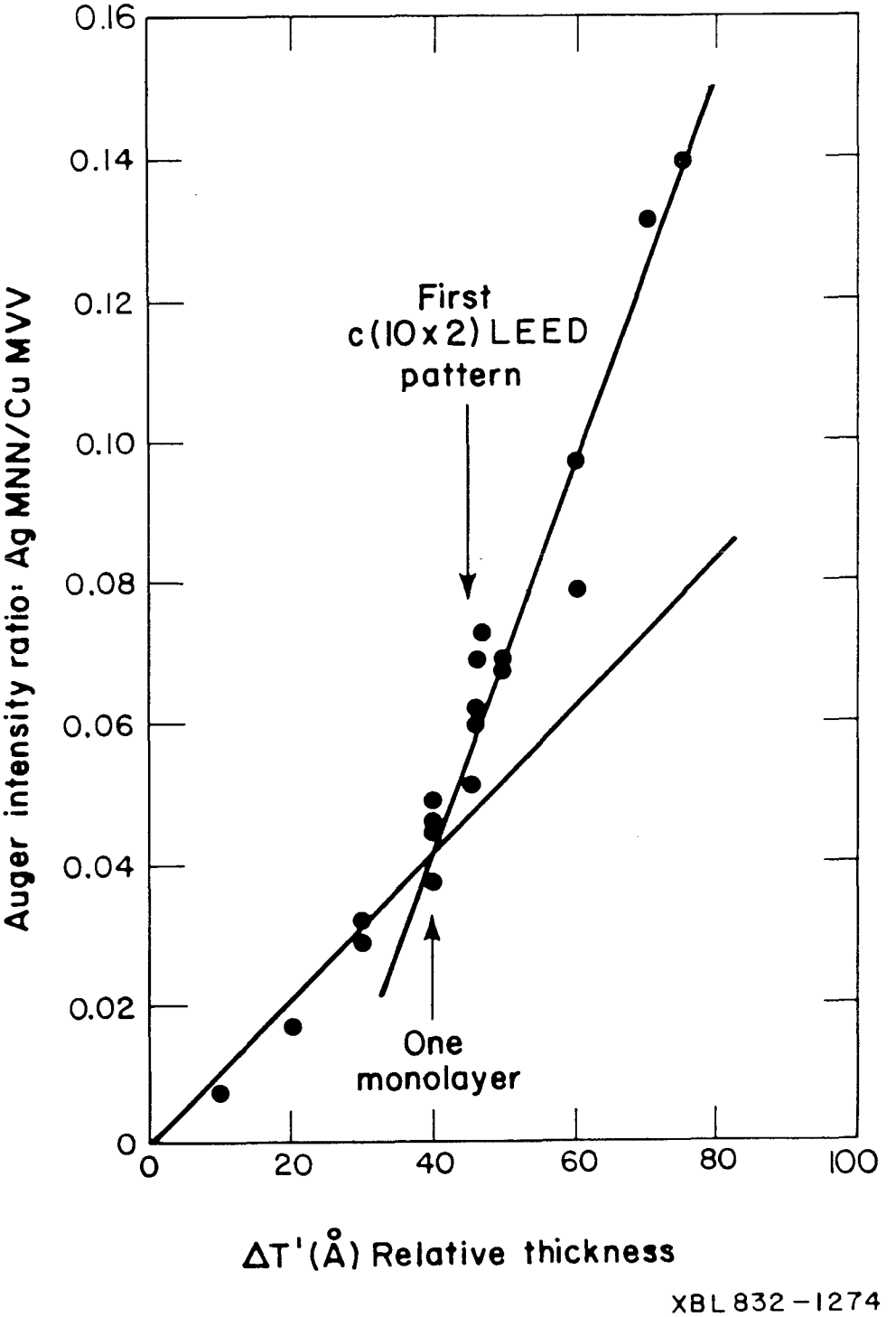
0.16
0.14
0.12
0.10
0.08
0.06
0.04
0.02
0
Auger intensity ratio: Ag MNN/Cu MVV
First
c(10x2) LEED
pattern
One
monolayer
0
20
40
60
80
100
ΔT'(Å) Relative thickness
XBL 832-1274

Figure 2

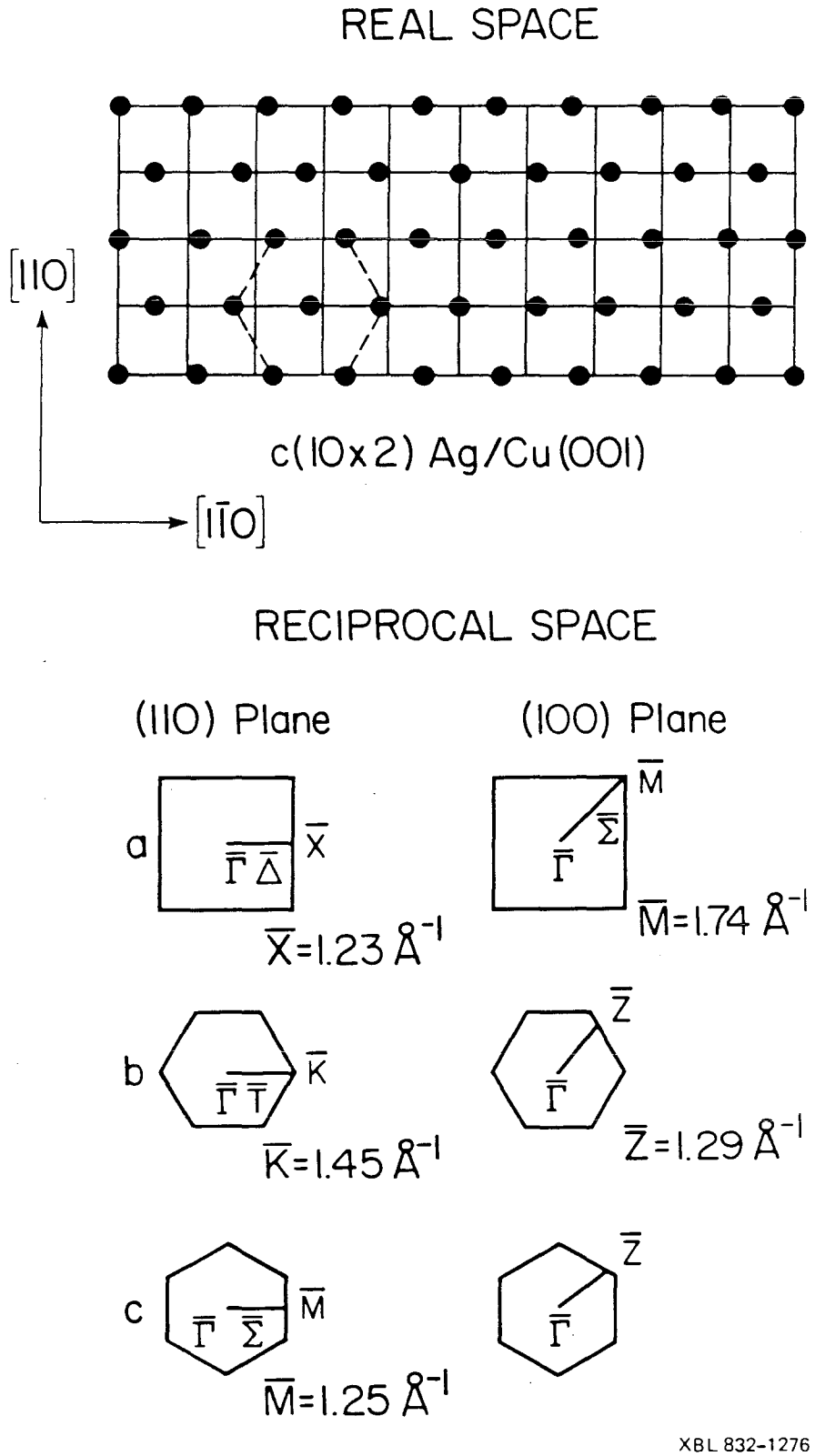
REAL SPACE
[110]
[1$\bar{1}$0]
c(10x2) Ag/Cu(001)
RECIPROCAL SPACE
(110) Plane
(100) Plane
a
$\bar{\Gamma}$ $\bar{\Delta}$
$\bar{X}$
$\bar{X}$=1.23 Å^{-1}
$\bar{\Gamma}$ $\bar{\Sigma}$
$\bar{M}$
$\bar{M}$=1.74 Å^{-1}
b
$\bar{\Gamma}$ $\bar{T}$
$\bar{K}$
$\bar{K}$=1.45 Å^{-1}
$\bar{\Gamma}$
$\bar{Z}$
$\bar{Z}$=1.29 Å^{-1}
c
$\bar{\Gamma}$ $\bar{\Sigma}$
$\bar{M}$
$\bar{M}$=1.25 Å^{-1}
$\bar{\Gamma}$
$\bar{Z}$
XBL 832-1276

Figure 3

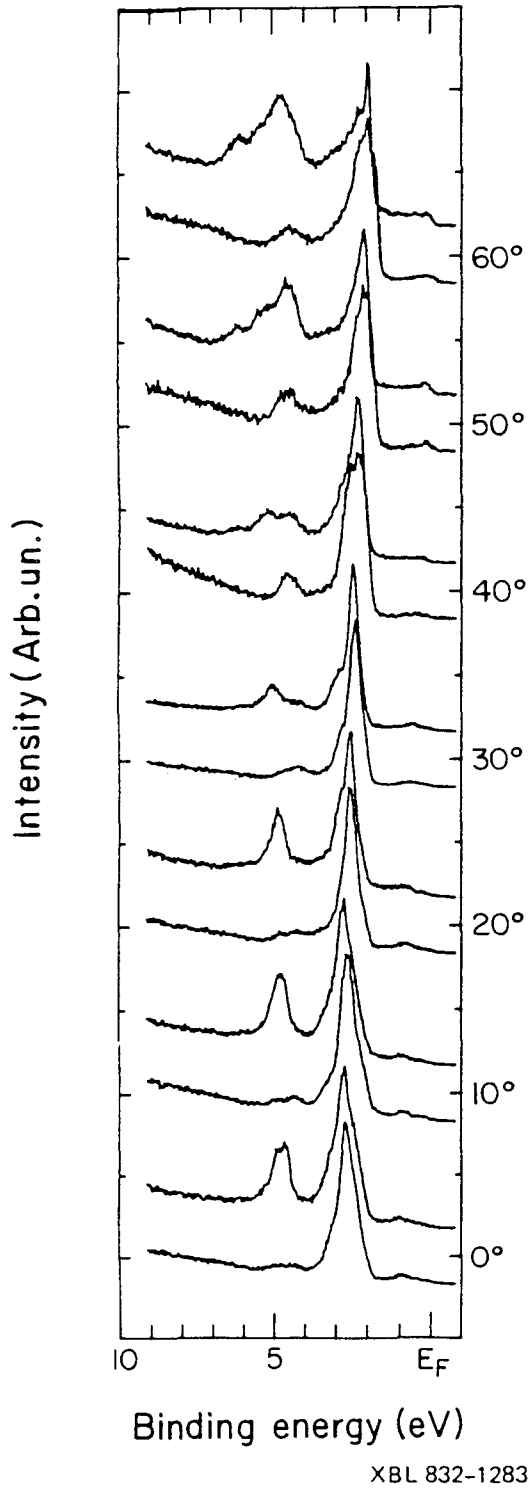
HeI S-Pol <100>
Intensity (Arb.un.)
60°
50°
40°
30°
20°
10°
0°
10
5
E_F
Binding energy (eV)
XBL 832-1283

Figure 4

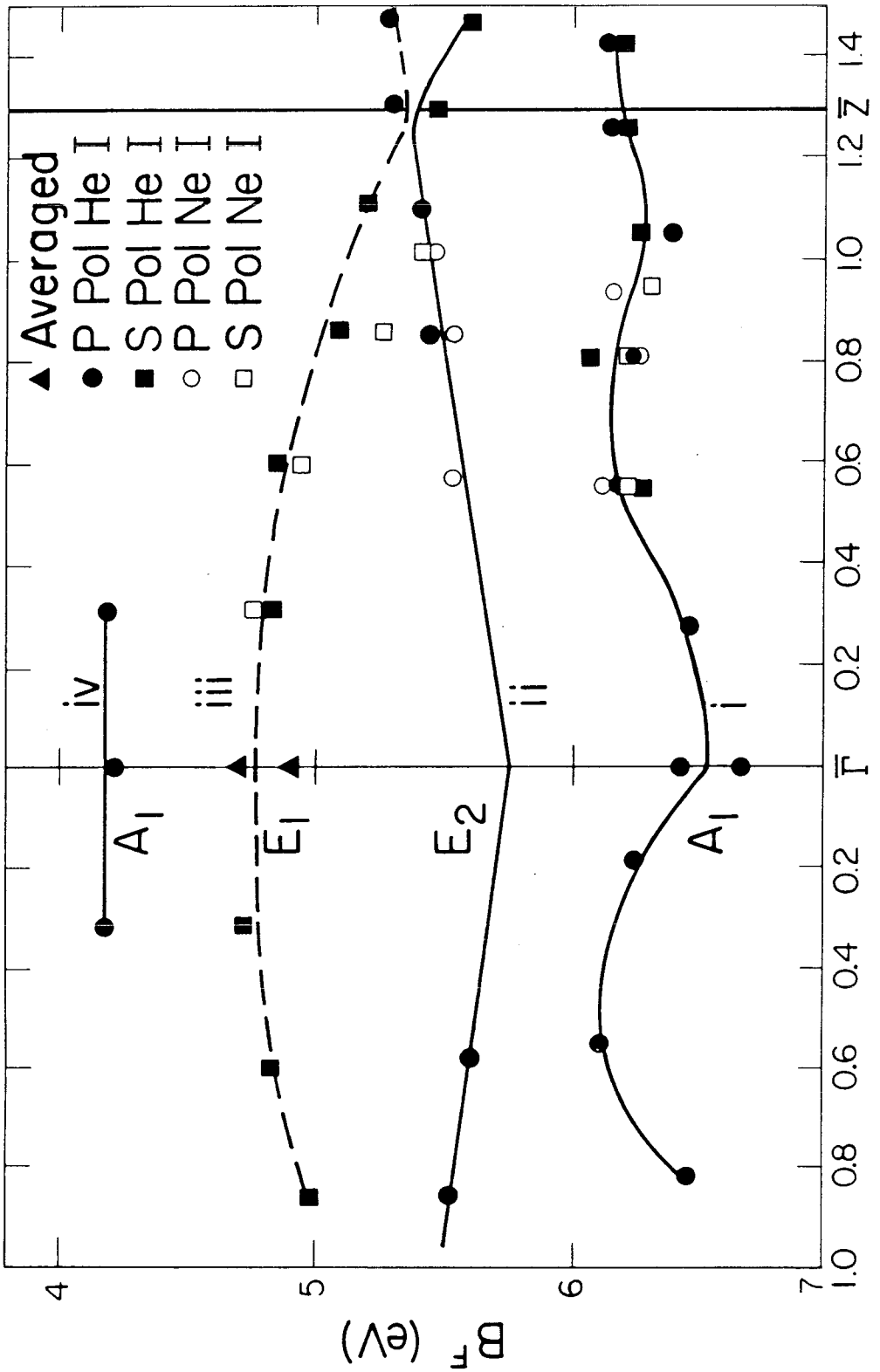
Averaged
P Pol He I
S Pol He I
P Pol Ne I
S Pol Ne I
iv
iii
ii
i
A_1
E_1
E_2
A_1
$\bar{\Gamma}$
$\bar{Z}$
B^{Γ} (eV)
$k_{\parallel}$ ($\AA^{-1}$) <110>
$k_{\parallel}$ ($\AA^{-1}$) <100>
XBL 832-1272B

Figure 5

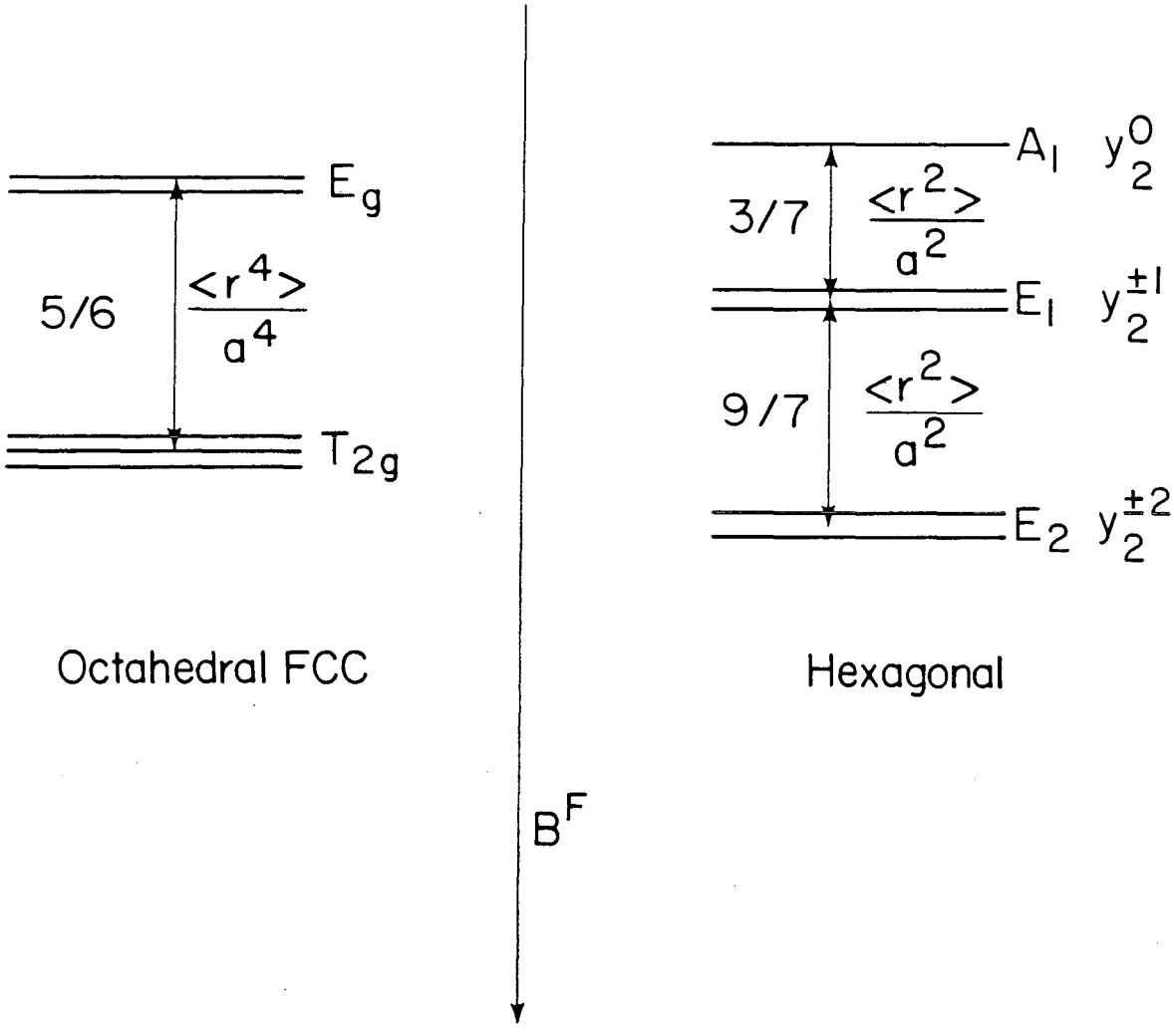

XBL 832-1277

Figure 6